2020 American Control Conference
Denver, CO, USA, July 1-3, 2020

A RULE-BASED DAMPING CONTROL OF MMR-BASED ENERGY-HARVESTING VEHICLE SUSPENSION

Qiuchi Xiong, Bonan Qin, Xiaofan Li, Lei Zuo

Department of Mechanical Engineering, Virginia Tech, Blacksburg, VA, USA (leizuo@vt.edu)

***Abstract*—Traditional shock absorbers dissipate large amount of vibration energy into heat waste via viscous oil dampers. To harvest such energy and improve the vehicle suspension performance, a novel energy-harvesting shock absorber that uses a mechanical motion rectifier (MMR) is introduced with a rule-based controller to improve vehicle ride comfort as well as harvested energy under the random road excitations with different roughness classes. The ride comfort performance of the controlled MMR shock absorber with rule-based strategy is compared with the passive shock absorber, the controlled traditional shock absorber with skyhook strategy, and the controlled MMR shock absorber with SH-PDD (skyhook-power driven damper) strategy. The rule-based MMR shock absorber shows the best ride comfort performance.**

I. INTRODUCTION

Suspensions play an important role in mitigating vehicles' vibration induced by road irregularities to achieve increased ride comfort and enhanced road handling. In conventional suspensions, large amount of vibration energy is dissipated into waste heat by the oil damper. Only 10-16% energy can be transformed into driving kinetic energy to overcome the resistance from road friction and air drag (DOE and EPA data). An average 100–400W power potential is available from the shock absorbers of a typical middle-sized passenger car at 60mph on the good (Class B) and average (Class C) roads [1].

To save the waste energy aforementioned and improve suspension performances simultaneously, energy-harvesting shock absorbers attract wide attentions in the past two decades. The earliest research on the linear regenerative electromagnetic shock absorbers (LESAs) were proposed by Karnopp [2], Fodor and Redfield [3], etc. A linear electromagnetic motor was utilized and produced a back electromotive force attenuating the suspension vibration. The energy-harvesting efficiency for LESAs is generally high, even up to 70%-78% [4]. However, the power density is too small, a retrofit design can only provide damping of 940 Ns/m under a short circuit condition [4], which is not sufficient for a compact-size passenger car.

To overcome such low-damping defects, the rotary regenerative shock absorbers have been proposed by utilizing some mechanisms, such us ball-screw mechanism [5,6], rack-pinion mechanism [7], hydraulic transmission [8,9] or some other motion conversion mechanisms [10,11], to convert linear suspension motion into rotation movements of generators. Graves et al. [12] demonstrated that the rotary electromagnetic module can significantly amplify the damping force and regeneration efficiency due to the transmission gear ratio. Li et al. [7] designed a rack-pinion based shock absorber and established the bench tests and road tests. The investigated suspension has a good power density and damping range of 1800Ns/m-8000Ns/m, but with a relatively low energy-harvesting efficiency 33%-56%. Such low energy-harvesting efficiency is mainly caused by the reciprocating suspension vibration being converted into bidirectional rotation of the generator [13].

To address this issue, mechanical motion rectifier (MMR)-based regenerative electromagnetic shock absorbers have been developed to convert reciprocating linear vibration into the unidirectional rotation of generators and produce a stable voltage with small ripples. Li et al. [14] developed an MMR shock absorber by using rack-pinion, bevel gears and one-way clutches. It increases the energy harvesting efficiency to around 60% with a greatly reduced backlash effect. However, the backlash still exists between the rack and pinion. Liu et al. [15] proposed an MMR-based energy harvesting shock absorber using a ball-screw mechanism with a mechanical efficiency up to 70%. Much smaller backlash also achieved than the rack-pinion design [14].

Although many types of regenerative electromagnetic shock absorbers have been developed, the research about the control of the regenerative electromagnetic shock absorber is not widely explored yet. For conventional suspension system, after first proposed by Karnopp et al. in 1974 [16], the semi-active suspension has been widely studied as a mean to provide better tradeoffs between performances and costs than passive or active control method. In order to improve ride comfort, Sky-Hook (SH) [17], Acceleration-Driven-Damper (ADD) [18] and the mixed SH and ADD (SH-ADD) [19], have been proposed to reduce the acceleration of the sprung mass, while some algorithms also try to enhance the road handling, such as Ground-Hook (GH) [20]. There are also many modern control algorithms in which both ride comfort and road handling are considered, such as hybrid model predictive control (HMPC) [21] and Linear Parameter Varying (LPV) [22].

However, for the MMR shock absorbers, two one-way clutches have been applied to achieve the conversion from bidirectional motion into unidirectional rotation of the generator. The one-way clutch will cause disengagement when the input shaft speed is lower than the output shaft speed. In such a case, the generator will be decoupled from the shock absorber, in which the vehicle dynamics will change. The MMR is considered as a piecewise linear system

978-1-5386-8266-1/$31.00 ©2020 AACC

with nonlinear behavior during disengagement. Currently, there is no control strategy that considers such disengagement to fully make use of the engagement and disengagement of the MMR for vehicle ride comfort improvement.

In this paper, a rule-based control strategy that considers the control performance of the engagement and disengagement at each time step on the MMR-based shock absorber is proposed. The control strategy compares the performance of the possible engagement/disengagement conditions to determine if the system should be engaged by using combined generator speed control and damping control. With the advantage of the MMR-based ball-screw mechanism, the available damping range has also been greatly extended. The rule-based control strategy is compared with existing power flow skyhook control on a traditional shock absorber with limited damping tuning capability, and also with existing SH-PDD control strategy that only considers engagement period of the MMR shock absorber. The rule-based control strategy achieves best ride comfort improvement among all of the compared controls.

The paper is organized as follows: Section II presents the design and modeling of the MMR shock absorber; in Section III, the skyhook control problem is formulated based on traditional shock absorber; in Section IV, the SH-PDD control problem is formulated based on MMR-based shock absorber; in Section V, the rule-based control problem is formulated based on MMR-based shock absorber; in Section VI, a case study and results are provided for control performance verification; the conclusion is given in Section VII.

II. Review of MMR Shock Absorber Design and Modeling

2.1 Design of the MMR-based Shock Absorber

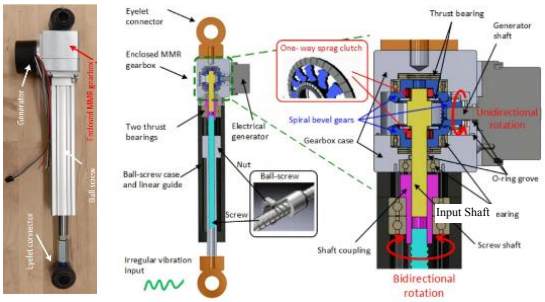

Fig 1. MMR-based Shock Absorber Design

In this section, the design and working principle of the MMR-based shock absorber will be briefly reviewed. The major innovation of the MMR design is to convert the bi-directional vibration of the suspension into unidirectional rotation of the generator to greatly improve system energy harvesting capability. With the MMR gearbox, an engageable equivalent inerter can also contribute to the ride comfort improvement. Fig. 1 shows the design of the MMR-based shock absorber. In the design, the conventional hydraulic chamber is replaced by a MMR gearbox driven by a ball-screw. The generator is driven by the output shaft of the MMR gearbox on the side. When the suspension deflects, a nut inside the shock absorber will have bi-directional vibration, which will drive the ball-screw to convert vertical motion into rotational motion. Then, the ball screw will drive the input shaft of the MMR gearbox at the bottom. Inside the gearbox, there are two bevel gears connected with two one-way clutches installed in opposite direction. A third bevel gear is connected with the generator shaft on the side of the gearbox. A one-way clutch can be locked in one direction (engage) and freely rotate in the other direction (disengage). Through the engagement and disengagement of these two one-way clutches, the generator will only rotate in one direction no matter which direction the input shaft rotates. The lab and field tests of such MMR based shock absorber can be seen in our paper [15].

2.2 Modeling of the MMR-based Shock Absorber

The modeling of the MMR-based shock absorber is summarized based on [15] and [24]. In Fig 2, a schematic diagram of the MMR-based shock absorber is shown.

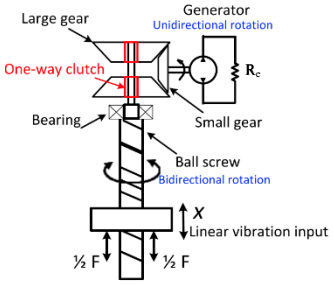

Fig 2. Schematic Diagram of the MMR-based Shock Absorber

In Fig 3, the simplified quarter car dynamic model during engagement and disengagement period is shown.

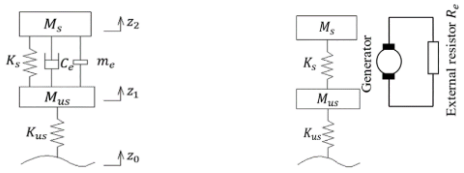

(a) Engage (b) Disengage

Fig 3. Dynamic Modeling of the MMR-based Shock Absorber

As shown in Fig 3(a), the engaged model of the suspension system will introduce a set of equivalent damping C_e, and equivalent inerter m_e resulted from the MMR gearbox components and the generator circuit.

$$M_s\ddot{z}_2 = K_s(z_1 - z_2) + m_e(\ddot{z}_1 - \ddot{z}_2) + C_e(\dot{z}_1 - \dot{z}_2), \dot{\theta} = \left|\dot{\theta}_{in}\right| \quad (1)$$

$$M_{us}\ddot{z}_1 = K_{us}(z_0 - z_1) - K_s(z_1 - z_2) - m_e(\ddot{z}_1 - \ddot{z}_2) - C_e(\dot{z}_1 - \dot{z}_2), \dot{\theta} = \left|\dot{\theta}_{in}\right| \quad (2)$$

where M_s is the sprung mass, M_{us} is the unsprung mass, z_1 is the unsprung mass displacement, z_2 is the sprung mass displacement; z_0 is the road input, K_s is the shock absorber stiffness, K_{us} is the tire stiffness, $\dot{\theta}$ is the rotating speed of the output shaft, and $\dot{\theta}_{in}$ is the rotational speed of the input shaft.

During the engagement period, the generator will be driven by the input shaft, therefore, results in same rotational speed. In the internal dynamic of the MMR gearbox and generator system, an external resistor, R_e is connected with the generator in series. The equivalent linear damping can be described as a function of the external resistor as below:

$$m_e = \frac{2(r_b^2 r_g^2 J_m + r_b^2 J_{sg} + 2J_{lg} + J_{bs})(\pi d_m + fl)}{(l - \pi f d_m) d_m l} \quad (3)$$

$$C_e = \frac{2r_b^2 r_g^2 (\pi d_m + fl)}{(l - \pi f d_m) d_m l} \left(\frac{3k_t k_e}{2(R_i + R_e)} + c_v\right) \quad (4)$$

where r_b is the gear ratio between the large bevel gear and the small bevel gear on the side of the gearbox, r_s is the generator gearhead ratio; J_m, J_{sg}, J_{lg}, and J_{bs} are the inertia of the

generator, small bevel gear, large bevel gear and the ball-screw; d_m is the pitch diameter of the ball-screw; f is the ball-screw friction factor [15]; l is the screw lead; k_t and k_e are the generator torque constant and voltage constant; R_i is the generator internal resistance; R_e is the external resistance; c_v is the generator viscous rotational damping.

When the output shaft has a higher speed than the input shaft, disengagement will occur (Fig 3b). In such situation, the generator will be decoupled from the suspension system, which therefore eliminates the equivalent damping and inerter. However, with the purpose to provide accurate model, the inertia of the MMR gearbox is still included in the suspension model. Since the inertia of the MMR gearbox is small compared to the engaged equivalent inerter, it is not shown in Fig 3(b). Based on Newton's second law, the disengaged dynamic equation can be formulated as:

$$M_s\ddot{z}_2 = K_s(z_1 - z_2) + m_{e-dis}(\ddot{z}_1 - \ddot{z}_2), \dot{\theta} > \dot{\theta}_{in} \quad (5)$$

$$M_{us}\ddot{z}_1 = K_{us}(z_0 - z_1) - K_s(z_1 - z_2) - m_{e-dis}(\ddot{z}_1 - \ddot{z}_2), \dot{\theta} > \dot{\theta}_{in} \quad (6)$$

where

$$m_{e-dis} = \frac{2(r_b^2 J_{sg} + 2J_{lg} + J_{bs})(\pi d_m + fl)}{(l - \pi f d_m) d_m l} \quad (7)$$

where $m_{e\text{-}dis}$ is the inertia of the MMR gearbox.

Since the generator is decoupled from the suspension system, it forms a dynamic system itself with the external resistor, R_e as shown in equation (8):

$$J_m\ddot{\theta} + c_m\dot{\theta} = 0 \Rightarrow \dot{\theta} = e^{-\frac{c_m}{J_m}t} \quad (8)$$

$$c_m = \frac{3k_i k_e}{2(R_i + R_e)} + c_v = c_{ele} + c_v \quad (9)$$

where c_m is the total rotational damping produced by the generator, including electrical damping part c_{ele} and mechanical damping part c_v. The c_v can be determined from the open-loop circuit bench test of MMR-based shock absorber. The value is 0.0023N-s/m in our prototype [15]. The damping caused by resistance and viscous friction will let the generator decay exponentially during disengage period.

III. Skyhook Control of Traditional Shock Absorber

3.1 Modeling of the Traditional Shock Absorber

In this section, the traditional suspension quarter car model will be introduced with a fixed passive damping.

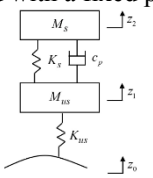

Fig 4. Dynamic Modeling of the Traditional Shock Absorber

Fig 4 shows the simplified quarter car model for the traditional shock absorber. The model has a constant suspension damping c_p selected based on maximum available MMR suspension damping. Based on Newton's second law, the dynamic equation can be written as:

$$M_s\ddot{z}_2 = K_s(z_1 - z_2) + c_p(\dot{z}_1 - \dot{z}_2) \quad (10)$$

$$M_{us}\ddot{z}_1 = K_{us}(z_0 - z_1) - K_s(z_1 - z_2) - c_p(\dot{z}_1 - \dot{z}_2) \quad (11)$$

3.2 Skyhook (SH) Control Formulation

Skyhook is a widely applied control strategy developed for semi-active suspension (shock absorber damping can be changed). Its main idea is to virtually create an ideal suspension system in which the chassis is "hooked" to a virtual inertial frame called "sky" by a passive damper c_{sky},

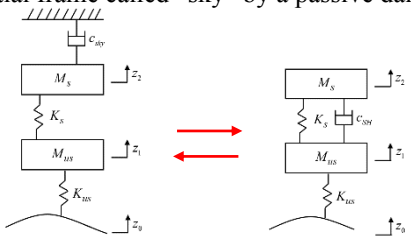

Fig 5. Skyhook Control Concept

then using the real suspension with an electromagnetic semi-active damper to emulate the dynamics of this ideal suspension system. The purpose of the control algorithm is to dissipate as much energy as possible from sprung mass to unsprung mass to improve vehicle ride comfort. The simplest skyhook control strategy only considers two damping stages, minimum damping c_{min} and maximum damping c_{max}. The control law can be concluded as [17]:

$$c_{SII}(t) = \begin{cases} c_{\max}, \ if \ (\dot{z}_2 - \dot{z}_1)\dot{z}_2 \geq 0 \\ c_{\min}, \ if \ (\dot{z}_2 - \dot{z}_1)\dot{z}_2 < 0 \end{cases} \quad (12)$$

IV. SH-PDD Control of MMR-based Shock Absorber

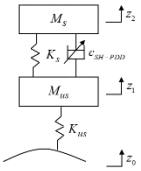

Fig 6. SH-PDD Control Concept

Another effective control strategy developed in [25] is also included as the baseline controller to evaluate the rule-based control strategy. It is a combination of SH and PDD strategy. The control concept is to choose large damping value when the damper absorbs energy from sprung mass, and choose small damping value when energy flows from damper to sprung mass. In the energy aspect, the SH-PDD method tries to extract as much energy as possible from the sprung mass and considers the balance the energy flowing into the suspension. The control law is developed as:

$$c_{e-SH-PDD}(t) = \begin{cases} c_{\max}, \ if \ \dot{z}_2^2 - \dot{z}_1^2 \geq 0 \text{ or } K_s(z_2 - z_1)(\dot{z}_2 - \dot{z}_1) + c_{\max}(\dot{z}_2 - \dot{z}_1)^2 < 0 \\ c_{\min}, \ if \ \dot{z}_2^2 - \dot{z}_1^2 < 0 \text{ and } K_s(z_2 - z_1)(\dot{z}_2 - \dot{z}_1) + c_{\min}(\dot{z}_2 - \dot{z}_1)^2 \geq 0 \\ \frac{-K_s(z_2 - z_1)}{(\dot{z}_2 - \dot{z}_1)}, \ otherwise \end{cases} \quad (13)$$

V. Rule-based Control of MMR-based Shock Absorber

When we apply the SH-PDD control strategy to MMR system, it can be seen that the damping control can only be effective during the engagement period, through changing the external resistance of the electric circuit (Eq. 4). However, during disengagement, generator is decoupled and is not able to adjust suspension dynamics. Therefore, a new control strategy that considers both the engagement and disengagement is proposed here.

From the modeling of the MMR shock absorber, when the generator speed is higher than the input shaft speed, the generator will be disengaged. Hence, by increasing generator speed to a higher value than the input shaft speed, system will be disengaged. During the disengagement, by changing system damping to a large value, the generator speed will decay faster to be engaged again with the shock absorber.

Therefore, by controlling generator speed as well as damping, system engagement can be controlled. However, in this paper, for simplification the dynamic of engagement/ disengagement control is ignored. In the control model, we assume that the engagement can be controlled instantly. The MMR system is a piecewise linear system that will switch system dynamics according to the speed comparison between the input shaft and generator speed. A global optimization method is hard to be formulated. Therefore, we formulated an instant optimization method that compares the instant power of the engagement and disengagement model at each time step in discretized manner.

Based on the MMR shock absorber dynamic equations, the state-space model during engage and disengage periods are formulated as:

Engage model,

$$\begin{pmatrix} \dot{z}_2-\dot{z}_1 \\ \ddot{z}_2 \\ \dot{z}_1-\dot{z}_0 \\ \ddot{z}_1 \end{pmatrix} = \begin{pmatrix} 0 & 1 & 0 & -1 \\ \frac{K_s m_e}{M_{us}-m_e}-K_s & \frac{m_e C_e}{M_{us}+m_e}-C_e & \frac{-m_e K_{us}}{M_{us}+m_e} & C_e-\frac{m_e C_e}{M_{us}+m_e} \\ M_s+m_e-\frac{m_e^2}{M_{us}+m_e} & M_s+m_e-\frac{m_e^2}{M_{us}+m_e} & M_s+m_e-\frac{m_e^2}{M_{us}+m_e} & M_s+m_e-\frac{m_e^2}{M_{us}+m_e} \\ 0 & 0 & 0 & 1 \\ K_s-\frac{K_s m_e}{M_s+m_e} & C_e-\frac{m_e C_e}{M_s+m_e} & -K_{us} & \frac{m_e C_e}{M_s+m_e}-C_e \\ M_{us}+m_e-\frac{m_e^2}{M_s+m_e} & M_{us}+m_e-\frac{m_e^2}{M_s+m_e} & M_{us}+m_e-\frac{m_e^2}{M_s+m_e} & M_{us}+m_e-\frac{m_e^2}{M_s+m_e} \end{pmatrix} \begin{pmatrix} z_2-z_1 \\ \dot{z}_2 \\ z_1-z_0 \\ \dot{z}_1 \end{pmatrix} + \begin{pmatrix} 0 \\ 0 \\ -1 \\ 0 \end{pmatrix} (\dot{z}_0) \quad (14)$$

Disengage model,

$$\begin{pmatrix} \dot{z}_2-\dot{z}_1 \\ \ddot{z}_2 \\ \dot{z}_1-\dot{z}_0 \\ \ddot{z}_1 \end{pmatrix} = \begin{pmatrix} 0 & 1 & 0 & -1 \\ \frac{K_s m_{e-dis}}{M_{us}-m_{e-dis}}-K_s & 0 & \frac{-m_{e-dis}k_{us}}{M_{us}+m_{e-dis}} & 0 \\ M_s+m_{e-dis}-\frac{m_{e-dis}^2}{M_{us}+m_{e-dis}} & 0 & M_s+m_{e-dis}-\frac{m_{e-dis}^2}{M_{us}+m_{e-dis}} & 0 \\ 0 & 0 & 0 & 1 \\ K_s-\frac{K_s m_{e-dis}}{M_s+m_{e-dis}} & 0 & -K_{us} & 0 \\ M_{us}+m_{e-dis}-\frac{m_{e-dis}^2}{M_s+m_{e-dis}} & 0 & M_{us}+m_{e-dis}-\frac{m_{e-dis}^2}{M_s+m_{e-dis}} & 0 \end{pmatrix} \begin{pmatrix} z_2-z_1 \\ \dot{z}_2 \\ z_1-z_0 \\ \dot{z}_1 \end{pmatrix} + \begin{pmatrix} 0 \\ 0 \\ -1 \\ 0 \end{pmatrix} (\dot{z}_0) \quad (15)$$

Then, the system is discretized by sample time T_s with first order hold for better approximation. At time k, the Fig 7 shows the logic flow of the rule-based control strategy:

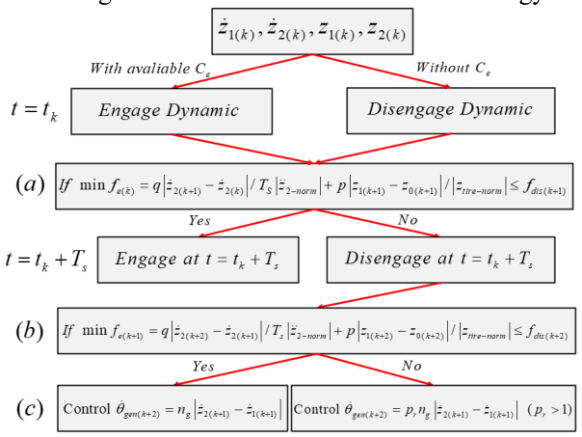

Fig 7. Control Logic of the Rule-based Control Strategy (a) 1st time step ride performance comparison (b) 2nd time step ride performance comparison (c) Generator speed control

In the logic figure, n_g is the combined gear ratio between the suspension deflection and the generator speed. The p_r is a coefficient of a value greater than 1 that ensures the generator speed will be controlled to be higher than the input shaft speed to cause disengagement.

At each time step, the control strategy will compare the instant vehicle body acceleration for both engage and disengage models for two time steps in the future. The available equivalent damping range will be divided with certain grid size. The control strategy will find the optimal damping value that minimize vehicle body acceleration.

The vehicle ride comfort index can be expressed as [26]:

$$a_{rms} = \sqrt{\frac{\frac{1}{N}\sum_{i=1}^{N}\ddot{z}_2(i)^2}{\frac{1}{N}\sum_{i=1}^{N}\ddot{z}_0(i)^2}}, i = 1,2,...,N \quad (16)$$

Therefore, the control algorithm targets on reducing instant vehicle body acceleration.

The vehicle road handling index is also considered as [26]:

$$\mu_{rms} = \frac{K_{us}\sqrt{\frac{1}{N}\sum_{i=1}^{N}(z_1(i)-z_0(i))^2}}{(M_s+M_{us})g}, i = 1,2,...,N \quad (17)$$

From the equation, it's easy to see that by reducing the instant tire deflection, the road handling index can be reduced.

By combining the ride comfort and road handling optimization, a cost function is formulated:

$$f_{e(k)} = q\left|\dot{z}_{2(k+1)} - \dot{z}_{2(k)}\right| / T_S \left|\ddot{z}_{2-norm}\right| + p\left|z_{1(k+1)} - z_{0(k+1)}\right| / \left|z_{tire-norm}\right| \quad (18)$$

where q and p are the weighting values for ride comfort and road handling performances. Since the cost function is normalized, the summation of q and p values equal to 1. The values of q and p are provided in the Table 1. We choose the value q is greater than p, since ride comfort performance is more important. The subscript k+1 means state value at $t = k+1$; $\ddot{z}_{2-norm}, z_{tire-norm}$ are the vehicle body acceleration and tire deflection for passive traditional shock absorber at the same time step. The passive traditional model is chosen as the baseline for all controlled models. Therefore, the normalization of the cost function is based on it.

In the engaged model, since different damping values can be applied, the minimum value of the cost function at each time step needs to be found.

Then, the minimum cost function value for engage model will be compared to the cost function value of disengage model to determine which mode can result in smaller vehicle body acceleration and dynamic tire load. The engagement at time $t = k$+1will also affect the dynamics of engagement at $t = k$+2. Therefore, the control strategy will process comparison for two time steps in the future at each time step.

VI. Case Study and Result Discussion

6.1 Road Profile Input

In order to justify control performance, a stochastic road profile with changing road grades classified by ISO 8608 [23] is considered as the road input for the simulation.

The road elevation PSD has a form:

$$G_d(n) = G_d(n_0)\left(\frac{n}{n_0}\right)^{-w} \quad (19)$$

Where $G_s(n)$ is unevenness index, w is waviness, n_0 is reference spatial frequency and n is spatial frequency. The road class parameters for different classes are displayed in Table 2. The road profile changes from class B road to class C road. The road profile is shown in Fig 8.

Table 2. Road roughness levels classified by ISO 8608

Road Class	Geometric mean $G_d(n_0)$ $(\times 10^{-6})m^3$, $n_0 = 0.1m^{-1}$
A	16
B	46
C	256

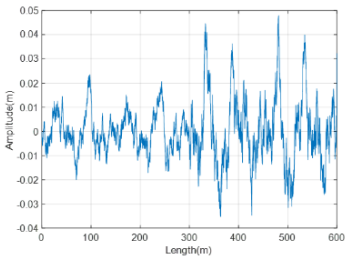

Fig 8. Ground Profile Input for B-class + C-class Road

6.2 Vehicle Parameters

A heavy-duty pickup truck (eg. Ford F250) quarter car model is applied as the target vehicle for simulation. Table 1 shows parameters applied in the simulation of the vehicle model. The gear ratio, r_b, between the large bevel and the small bevel gears on the side is optimized for minimum vehicle body acceleration for the passive MMR, as shown in Fig 9. The simulation is done in time domain with the consideration of the MMR feature for the road profile input. It can be seen that the lowest point in the plot gives a r_b =0.9. Such value r_b and external resistance R_e determine the damping range of MMR shock absorber.

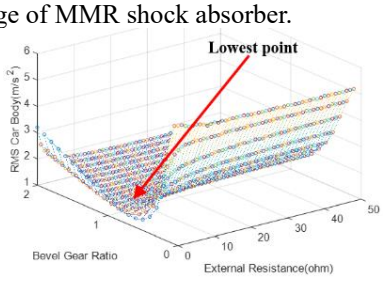

Fig 9. 3-D Plot to Determine Optimal Gear Ratio r_b

Table 1. Vehicle and Suspension Parameters

Name	Symbol	Value	Unit
Sprung mass	M_s	575	*kg*
Unsprung mass	M_{us}	265	*kg*
Suspension stiffness	K_s	125	*kN/m*
Tire stiffness	K_{us}	750	*kN/m*
Traditional shock absorber damping	c_p	7.9	*kN-s/m*
Vehicle speed	v	18	*m/s*
Ball-screw pitch diameter	d_m	0.008	*m*
Ball-screw lead	l	0.006	*m*
Ball-screw friction factor	f	0.15	
Generator inertia	J_m	$1.21 \cdot 10^{-4}$	*kg-m²*
Large bevel gear inertia	J_{lg}	10^{-5}	*kg-m²*
Small bevel gear inertia	J_{sg}	$6.5 \cdot 10^{-7}$	*kg-m²*
Ball-screw inertia	J_{bs}	$2 \cdot 10^{-6}$	*kg-m²*
Gear ratio between large bevel gear and small bevel gear	r_b	0.9	
Generator gearhead ratio	r_g	1	
Generator voltage constant	k_e	0.114	*V/rad*
Generator torque constant	k_t	0.114	*Nm/A*
Generator internal resistance	R_i	1.1	*ohm*
Generator viscous damping	c_v	0.0023	*N-s/m*
System gear ratio between input and output shafts	n_g	150	
External resistance	R_e	0:1:50	*ohm*
Simulation sample time	T_s	0.0056	*s*
Ride comfort weight	q	0.6	
Road handling weight	p	0.4	

In the simulation, the equivalent mechanical damping caused by c_v is 4.4kN-s/m. The external resistance R_e changes from 0 to 50 ohms. When increasing external resistance value, system equivalent damping will decrease. Therefore, the system corresponding equivalent electrical damping range is from 7.9kN-s/m to 1kN-s/m. However, because of the the mechanical damping 4.4kN-s/m, when furtherly increasing external resistance over 50 ohms, system total damping is not sensitive to resistance change anymore.

The passive traditional model uses maximum available damping of the MMR shock absorber as the constant damping of the system. For fair comparison, all controlled models will use same damping range as optimized passive MMR shock absorber.

6.3 Simulation Results

In this section will present the simulation results of the vehicle body acceleration for different models and power generation of energy harvesting shock absorber.

Fig 10 shows the control force comparison for skyhook, SH-PDD and rule-based controller. With same damping limits, the skyhook controller applies largest control force for most of the time, since it can only select control force between minimum and maximum damping forces. The SH-PDD controller has one more tuning value capability in damping compared to that of the skyhook control, which reduces control effort sometimes. The rule-based controller has the best damping tuning flexibility.

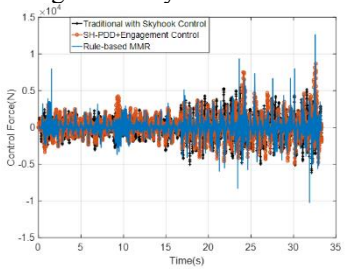

Fig 10. Control Force Comparison for All Controlled Models

Fig 11 shows the ride comfort comparison among passive traditional shock absorber, skyhook controlled traditional shock absorber, SH-PDD controlled MMR shock absorber and the rule-based MMR shock absorber. Note the original SH-PDD method does not consider MMR engagement in control. For fair comparison, the same logic to choose to engage or disengage at each time step is also applied to the SH-PDD method. It can be shown that the passive traditional shock absorber has the worst vehicle body acceleration under the same road excitation compared to controlled models. The skyhook performs better compared to the passive model, however, due to limited damping tuning options, it is worse than the rule-based MMR model. The SH-PDD method introduces another damping tuning value, however, it does not show noticeable improvement compared to skyhook method. Different from skyhook and SH-PDD methods, rule-based controller has various damping tuning capability that can change damping at each time step for minimum instant vehicle body acceleration. Therefore, it performs best among all control models, even with smallest damping force.

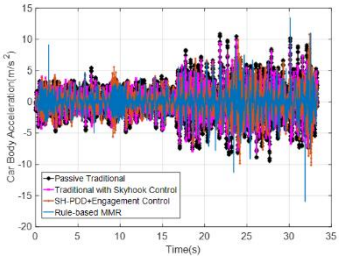

Fig 11. Ride Comfort Comparison among Different Models

Fig 12 shows the power generation for the controlled MMR shock absorber with SH-PDD and rule-based methods on generator electrical damping.

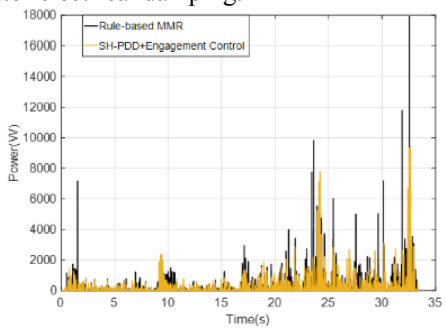

Fig 12. Power Generation for Controlled MMR Shock Absorber

The MMR model with fixed *Re* is also compared with passive traditional model with optimized bevel gear ratio, r_b, and external resistance, *Re*. The parameters of r_b *Re* are optimized based on Class B road. We also looked into other class roads and noticed that optimize the two parameters didn't change much.

Table 3 shows the rms value of vehicle body acceleration comparison for all models. The passive traditional shock absorber will be the baseline. The MMR shock absorber with fixed *Re* improves 16.7%. The skyhook control has 18.9% of improvement. The SH-PDD model has 19% improvement and the rule-based model has 29.2% improvement. Table 3. Comparison of Vehicle Ride Comfort and Power Harvesting

System	Ride comfort		Harvesting
	$\ddot{z}_{s-rms}(m/s^2)$	Improvement	Avg. Power (W)
Traditional absorber	2.528	0%	---
MMR with fixed *Re*	2.106	16.7%	137
Traditional + Skyhook control	2.050	18.9%	---
SH-PDD+Engagement control	2.048	19.0%	189
Rule-based	1.789	29.2%	187

VII. Conclusion

The paper introduced a rule-based control strategy designed for a mechanical motion rectifier (MMR) based energy harvesting shock absorber with the simulation on a quarter car model with pickup truck parameters. Passive traditional shock absorber, skyhook controlled traditional shock absorber, and SH-PDD controlled MMR shock absorber are compared with the proposed rule-based controller on ride comfort performance. The rule-based controller achieves the best performance (29.2%) in ride comfort compared to the passive traditional shock absorber, while the MMR shock absorber shows 16.7% improvement.

REFERENCES

[1] Zuo, L. and Zhang, P.S., 2013. Energy harvesting, ride comfort, and road handling of regenerative vehicle suspensions. Journal of Vibration and Acoustics, 135(1), p.011002.

[2] Karnopp, D., 1989. Permanent magnet linear motors used as variable mechanical dampers for vehicle suspensions. Vehicle System Dynamics, 18(4), pp.187-200.

[3] Fodor, M.G. and Redfield, R., 1993. The variable linear transmission for regenerative damping in vehicle suspension control. Vehicle System Dynamics, 22(1), pp.1-20.

[4] Tang, X., Lin, T. and Zuo, L., 2013. Design and optimization of a tubular linear electromagnetic vibration energy harvester. IEEE/ASME Transactions on Mechatronics, 19(2), pp.615-622.

[5] Kawamoto, Y., Suda, Y., Inoue, H. and Kondo, T., 2008. Electro-mechanical suspension system considering energy consumption and vehicle manoeuvre. Vehicle System Dynamics, 46(S1), pp.1053-1063.

[6] Cassidy, I.L., Scruggs, J.T., Behrens, S. and Gavin, H.P., 2011. Design and experimental characterization of an electromagnetic transducer for large-scale vibratory energy harvesting applications. Journal of Intelligent Material Systems and Structures, 22(17), pp.2009-2024.

[7] Li, Z., Zuo, L., Luhrs, G., Lin, L. and Qin, Y.X., 2012. Electromagnetic energy-harvesting shock absorbers: design, modeling, and road tests. IEEE Transactions on vehicular technology, 62(3), pp.1065-1074.

[8] Zou, J., Guo, X., Abdelkareem, M.A., Xu, L. and Zhang, J., 2019. Modelling and ride analysis of a hydraulic interconnected suspension based on the hydraulic energy regenerative shock absorbers. Mechanical Systems and Signal Processing, 127, pp.345-369.

[9] Chen, Y., Qin, B., Guo, S., Yu, L., and Zuo, L., 2019. Asymmetric energy harvesting and hydraulically interconnected suspension: modeling and validations. Proceedings of the IDETC/CIE California, ASME Paper No. IDETC2019-98402.

[10] Maravandi, A. and Moallem, M., 2015. Regenerative shock absorber using a two-leg motion conversion mechanism. IEEE/ASME Transactions on Mechatronics, 20(6), pp.2853-2861.

[11] Salman, W., Qi, L., Zhu, X., Pan, H., Zhang, X., Bano, S., Zhang, Z. and Yuan, Y., 2018. A high-efficiency energy regenerative shock absorber using helical gears for powering low-wattage electrical device of electric vehicles. Energy, 159, pp.361-372.

[12] Graves, K.E., Iovenitti, P.G. and Toncich, D., 2000. Electromagnetic regenerative damping in vehicle suspension systems. International Journal of Vehicle Design, 24(2-3), pp.182-197.

[13] Guo, S., Liu, Y., Xu, L., Guo, X. and Zuo, L., 2016. Performance evaluation and parameter sensitivity of energy-harvesting shock absorbers on different vehicles. Vehicle System Dynamics, 54(7), pp.918-942.

[14] Li, Z., Zuo, L., Kuang, J. and Luhrs, G., 2012. Energy-harvesting shock absorber with a mechanical motion rectifier. Smart Materials and Structures, 22(2), p.025008.

[15] Liu, Y., Xu, L. and Zuo, L., 2017. Design, modeling, lab, and field tests of a mechanical-motion-rectifier-based energy harvester using a ball-screw mechanism. IEEE/ASME Transactions on mechatronics, 22(5), pp.1933-1943.

[16] Karnopp, D., Crosby, M. and Harwood, R.A., 1974. Vibration control using semi-active suspension control. Journal of Engineering for Industry, 96, pp.619-626.

[17] Sammier, D., Sename, O. and Dugard, L., 2003. Skyhook and H_∞ control of semi-active suspensions: some practical aspects. Vehicle System Dynamics, 39(4), pp.279-308.

[18] Savaresi, S.M., Silani, E. and Bittanti, S., 2005. Acceleration-Driven-Damper (ADD): An optimal control algorithm for comfort-oriented semiactive suspensions. Journal of dynamic systems, measurement, and control, 127(2), pp.218-229.

[19] Savaresi, S.M. and Spelta, C., 2007. Mixed sky-hook and ADD: Approaching the filtering limits of a semi-active suspension. Journal of dynamic systems, measurement, and control, 129(4), pp.382-392.

[20] Valasek, M., Novak, M., Sika, Z. and Vaculin, O., 1997. Extended ground-hook-new concept of semi-active control of truck's suspension. Vehicle system dynamics, 27(5-6), pp.289-303.

[21] Giorgetti, N., Bemporad, A., Tseng, H.E. and Hrovat, D., 2006. Hybrid model predictive control application towards optimal semi-active suspension. International Journal of Control, 79(05), pp.521-533.

[22] Poussot-Vassal, C., Sename, O., Dugard, L., Gaspar, P., Szabo, Z. and Bokor, J., 2008. A new semi-active suspension control strategy through LPV technique. Control Engineering Practice, 16(12), pp.1519-1534.

[23] Mucka, P., 2017. Simulated road profiles according to ISO 8608 in vibration analysis. Journal of Testing and Evaluation, 46(1), pp.405-418.

[24] Li, X., Chen, C., 2018. Design and simulation of a novel mechanical power take-off for two-body wave energy point absorber. ASME, IDETC/CIE.

[25] Liu, Y., Zuo, L., 2016. Mixed skyhook and power-driven-damper: a new low-jerk semi-active suspension control based on power flow analysis. Journal of Dynamic Systems, Measurement, and Control, 138.

[26] Poussot-Vassal, C., Savaresi, S. M., 2010. A methodology for optimal semi-active suspension systems performance evaluation. Decision and Control (CDC), 49th IEEE Conference, pp. 2892-2897.